

# Measurement of interaction energy near a Feshbach resonance in a ${}^6\text{Li}$ Fermi gas

T. Bourdel<sup>1</sup>, J. Cubizolles<sup>1</sup>, L. Khaykovich<sup>1</sup>, K. M. F. Magalhães<sup>1</sup>,  
S. J. J. M. F. Kokkelmans<sup>1</sup>, G. V. Shlyapnikov<sup>1,2,3</sup>, and C. Salomon<sup>1</sup>

<sup>1</sup>Laboratoire Kastler Brossel, Ecole Normale Supérieure, 24 rue Lhomond, 75231 Paris 05, France

<sup>2</sup>FOM Institute AMOLF, Kruislaan 407, 1098 SJ Amsterdam, The Netherlands

<sup>3</sup>Russian Research Center Kurchatov Institute, Kurchatov Square, 123182 Moscow, Russia

(Dated: November 4, 2018)

We investigate the strongly interacting regime in an optically trapped  ${}^6\text{Li}$  Fermi mixture near a Feshbach resonance. The resonance is found at 800(40) G in good agreement with theory. Anisotropic expansion of the gas is interpreted by collisional hydrodynamics. We observe an unexpected and large shift (80 G) between the resonance peak and both the maximum of atom loss and the change of sign of the interaction energy.

PACS numbers: 34.90.+q, 05.30.Fk, 32.80.Pj, 05.20.Dd

The achievement of Bose-Einstein condensation (BEC) in dilute atomic gases [1] has naturally triggered research on cooling of Fermi gases to quantum degeneracy. Several groups have now reached Fermi degeneracy in  ${}^{40}\text{K}$  and  ${}^6\text{Li}$  with temperatures down to about 0.1 to 0.2 of the Fermi temperature  $T_F$  [2, 3, 4, 5, 6, 7]. One of the major goals of this research is to observe the transition to a superfluid phase [8], the analog of the superconducting (BCS) phase transition in metals [9]. Very low temperatures and strong attractive interactions in a two-component Fermi gas are favorable conditions to reach this superfluid state. The interactions in atomic gases at low temperature are usually described by a single parameter, the  $s$ -wave scattering length  $a$ . This quantity can be tuned near a Feshbach resonance where the sign and magnitude of  $a$  can be adjusted by means of an external magnetic field  $B$  [10, 11]. Therefore, when entering the regime of strong interactions, dilute Fermi gases offer unique opportunities to test new theoretical approaches. For instance, near resonance, the critical temperature for superfluidity has been predicted to be as high as  $0.25\text{-}0.5 T_F$  [12], a temperature range experimentally accessible.

Both  ${}^{40}\text{K}$  and  ${}^6\text{Li}$  possess Feshbach resonances at convenient magnetic fields [13, 14]. In Fig. 1 is plotted the theoretical scattering length for the mixture of the two lowest spin states of  ${}^6\text{Li}$ ,  $|F, m_F\rangle = |1/2, 1/2\rangle$ ,  $|1/2, -1/2\rangle$ , calculated from updated potentials consistent with the recently measured zero crossing of  $a$  at  $B \simeq 530$  G [15, 16]. Beside the broad resonance near 855 G on which we concentrate in this work, there is a very sharp resonance at 545 G, and increased atom losses have been measured peaking around 545 G and 680 G [5]. Recently, strong interactions in this Fermi mixture have been demonstrated at a fixed magnetic field of 930 G through anisotropic expansion of the gas [7]. In this Letter we study the atomic interactions through the entire range of the Feshbach resonance, from 600 G up to 1.3 kG. We measure three physical quantities: the interaction energy with positive and negative values, the anisotropy of the atomic cloud during the expansion, and the atom loss.

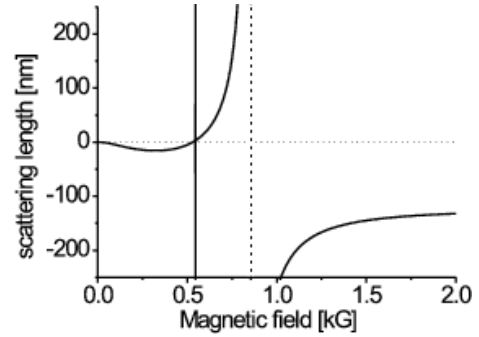


FIG. 1: Predicted scattering length *vs* magnetic field in  ${}^6\text{Li}$   $|F, m_F\rangle = |1/2, 1/2\rangle, |1/2, -1/2\rangle$  mixture.

We find the resonance at 800(40) G, where the trapped gas is most strongly interacting, with a ratio between the interaction energy and the kinetic energy reaching  $-0.3$ . Surprisingly, we observe a large shift ( $\sim 80$  G) between this position, and both the location of maximum loss in the gas and the change of sign of the interaction energy. Our results are in partial agreement with the physical picture of a Feshbach resonance in the region of strong interactions but also reveal unexpected effects. Finally they point towards the best experimental conditions to search for the superfluid transition in  ${}^6\text{Li}$ .

Our experimental approach to measure the interaction energy of a two component Fermi gas is based on the analysis of time of flight (TOF) images of atoms released from an anisotropic trap. The energy of the trapped gas, prepared at any value of the  $B$  field, is the sum of potential, kinetic and interaction energies,  $E_{pot} + E_{kin} + E_{int}$ . Switching off abruptly the trapping potential ( $E_{pot} \rightarrow 0$ ), the gas is released and expands for a variable time before an absorption image is recorded. At long expansion time, the spatial distribution of the cloud reflects the velocity distribution. This procedure is done routinely for BEC studies [1] and has been recently investigated theoretically for Fermi gases in [17]. The novelty of our approach is in what follows. Because of the low inductance of the coils used to produce the magnetic field  $B$ ,

this field can be switched off rapidly ( $\leq 20 \mu\text{s}$ ) at any desired time during the expansion of the atomic cloud. For  $B = 0$  the atoms have negligible interactions since  $a \simeq 0$  (Fig. 1). As a consequence, the expansion of the gas can be recorded without atomic interactions during the time of flight period ( $B = 0$ ), or with interactions during the TOF period ( $B \neq 0$ ). Since expansions with  $B = 0$  are ballistic, they reflect the kinetic energy of the initially trapped gas,  $E_{kin}$ . On the other hand, for TOF with  $B \neq 0$ , the interaction energy is converted into kinetic energy during the early stage of the expansion ( $\lesssim 150 \mu\text{s}$ ). TOF images at long time reflect the released energy,  $E_{rel} = E_{kin} + E_{int}$  [18]. Comparisons between TOF images with  $B = 0$  and  $B \neq 0$  allow us to simply deduce the ratio  $E_{int}/E_{kin}$ . We operate at temperatures between  $0.5 T_F$  and  $T_F$ , where Fermi degeneracy does not play an important role. Even in this nearly classical regime, the gas is found to be strongly interacting. The observed expansions with  $B \neq 0$  are anisotropic because of collisional hydrodynamics, as predicted in [19, 20], and observed in [7, 21, 22].

Our experimental setup has been described previously [4, 23]. A gas of  $3 \times 10^5$   $^6\text{Li}$  atoms is prepared in the absolute ground state  $|1/2, 1/2\rangle$  in a Nd-YAG crossed beam optical dipole trap at a temperature of  $10 \mu\text{K}$ . The horizontal beam (resp. vertical) propagates along  $x$  ( $y$ ), has a maximum power of  $2.5 \text{ W}$  ( $2.5 \text{ W}$ ) and a waist of  $\sim 25 \mu\text{m}$  ( $\sim 30 \mu\text{m}$ ). At full power the trap oscillation frequencies are  $\omega_x/2\pi = 2.2(2) \text{ kHz}$ ,  $\omega_y/2\pi = 3.0(3) \text{ kHz}$ , and  $\omega_z/2\pi = 3.7(4) \text{ kHz}$ , as measured by parametric excitation. Using a radio frequency field, we drive the Zeeman transition between  $|1/2, 1/2\rangle$  and  $|1/2, -1/2\rangle$  to prepare a balanced mixture of the two states at any chosen value of  $B$  between  $2 \text{ G}$  and  $1.3 \text{ kG}$ . Using a Stern-Gerlach method we check that the populations in both states are equal to within  $10\%$ .

We observe that atom losses occur with very different rates below and above resonance. Near  $720 \text{ G}$  the lifetime of the gas is on the order of  $10 \text{ ms}$ , whereas near  $900 \text{ G}$ , the lifetime is in excess of  $10 \text{ s}$ . The latter is surprisingly large in comparison with similar situations for bosons near a Feshbach resonance [24]. Therefore we performed two sets of experiments: one with the spin mixture prepared above resonance ( $1060 \text{ G}$ ), and the other below resonance ( $5 \text{ G}$ ). In the first set, evaporative cooling is performed by lowering the power of the vertical beam. It produces  $2N = 7 \times 10^4$  atoms at  $T \simeq 0.6 T_F$  with  $k_B T_F = \hbar \bar{\omega} (6N)^{1/3}$  and  $\bar{\omega} = (\omega_x \omega_y \omega_z)^{1/3}$ . The trap is nearly cigar shaped with frequencies  $\omega_x/2\pi = 1.1 \text{ kHz}$ ,  $\omega_y/2\pi = 3.0 \text{ kHz}$ , and  $\omega_z/2\pi = 3.2 \text{ kHz}$ . The magnetic field is adiabatically ramped in  $50 \text{ ms}$  to a final value where TOF expansion images are taken. The effect of strong interactions is illustrated in Fig. 2, where both typical images and a plot of the expanded cloud gaussian sizes  $r_x$  and  $r_y$  are displayed. In Fig. 2a, expansions with  $B = 0$  reveal the initial momentum distribution of

the cloud which is isotropic as expected. We deduce the total kinetic energy  $E_{kin}$  of the trapped gas mixture from gaussian fits to this distribution. For our moderate quantum degeneracy, the temperature can be estimated from  $k_B T = 2E_{kin}/3$ . We find  $T \simeq 3.5 \mu\text{K} \simeq 0.6 T_F$ , constant for fields between  $0.8 \text{ kG}$  and  $1.3 \text{ kG}$ .

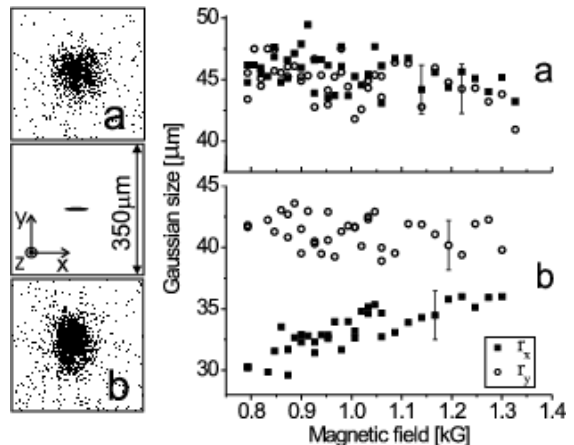


FIG. 2: Left: Geometry of the trapped atomic cloud (center) and expansion images without magnetic field (a) ( $B = 0$ ), and with magnetic field (b) ( $B \neq 0$ ). Right: Corresponding gaussian sizes of the expanded clouds along  $x$  (squares) and  $y$  (open circles) vs magnetic field. a : Time of flight images after  $650 \mu\text{s}$  expansion with  $B = 0$ . b: Images after  $400 \mu\text{s}$  expansion with  $B \neq 0$  and  $250 \mu\text{s}$  with  $B = 0$ . Images shown on the left are for  $B = 900 \text{ G}$ .

In Fig. 2b, expansions with  $B \neq 0$  are anisotropic. Little expansion is seen along the weak axis of the trap. The ellipticity of the cloud is inverted because of hydrodynamic behavior during the expansion [7]. Collisions then redistribute the gas energy in the direction of maximum density gradient. The anisotropy  $r_y/r_x$  ranges from  $1.1$  at large  $B$  field to  $1.4$  near  $0.8 \text{ kG}$  whereas the hydrodynamic scaling equations [19] predict an anisotropy of  $1.53$  in the fully hydrodynamic regime. The usual criterion for hydrodynamicity is found from the ratio  $R$  of the mean free path  $\lambda_0 = (n_0 \sigma)^{-1}$ , where  $n_0$  is the peak density, over the radial size  $r_{rad}$  of the cloud. For a classical gas neglecting mean field interactions we find:

$$R = \frac{\lambda_0}{r_{rad}} = \frac{(2\pi)^{3/2}}{N\sigma} \left( \frac{k_B T}{m\bar{\omega}^2} \right) \frac{\omega_{rad}}{\bar{\omega}}$$

$R \ll 1$  ( $R \gg 1$ ) corresponds to the hydrodynamic (collisionless) regime. With the predicted value of  $a = -185 \text{ nm}$  at  $1060 \text{ kG}$ , and  $\sigma = 4\pi a^2$ ,  $R = 0.03$ . Therefore in the early stages of the expansion, the gas is hydrodynamic as in [7, 21, 22]. Furthermore, with these large values of  $a$  and our typical temperatures, the scattering cross section is energy dependent. At  $B = 1060 \text{ G}$ ,  $|ka| = 0.95$ , where  $k = \sqrt{mk_B T/2\hbar^2}$  is the typical relative momentum of two colliding atoms. The cross section is reduced and becomes unitarity limited,  $\sigma = 4\pi a^2/(1 + k^2 a^2) \simeq$

$4\pi/k^2$  for  $|ka| \gg 1$  [26]. Consequently, as the magnetic field is decreased below 1.3kG, the gas gradually enters deeper in the unitarity regime.

This effect has an important consequence on the gas behavior during hydrodynamic expansion: since the relative momentum  $k$  of the colliding atoms decreases as  $k \propto n^{1/3}$  (where  $n$  is the density) [25],  $\sigma$  increases. For a spherical cloud, the hydrodynamic factor  $R$  would remain constant during expansion while for a cigar shaped cloud, the expansion is mostly 2D, and  $R$  decreases like  $n^{1/6}$ . The gas becomes more hydrodynamic as the expansion proceeds until this model breaks down when relative momenta  $k$  become too small to remain in the unitarity limit [27]. Then  $R$  increases as  $n^{-2/3}$  for a spherical geometry, and as  $n^{-1/2}$  for a cigar. Consequently, the larger  $|a|$ , the longer the expansion remains hydrodynamic and the stronger the anisotropy is. When the  $B$  field is decreased in Fig. 2, the anisotropy increase indicates that the scattering length becomes more and more negative. Therefore, this puts an upper bound of  $\simeq 800$  G for the position of the Feshbach  $s$ -wave resonance.

In the second set of experiments, we focused on the lower magnetic field values between 550 G and 820 G, the region where losses have been observed. The mixture is prepared at low magnetic field, and the field is ramped up to 320 G, where the scattering length  $vs$   $B$  has a local minimum of  $a = -8$  nm. Evaporative cooling is performed there, leading to  $T = 2.4 \mu\text{K}$  and to  $\omega_x/2\pi = 0.78$  kHz,  $\omega_y/\pi = 2.1$  kHz, and  $\omega_z/2\pi = 2.25$  kHz. Finally, the  $B$  field is ramped to 555 G in 50 ms where  $a \simeq 0$ , and then in 10 ms to different values between 600 G and 850 G where TOF expansions are recorded. The gaussian widths and number of detected atoms  $vs$   $B$  are plotted in Fig. 3. Comparing with the data of Fig. 2, we observe several new features. First, the number of detected atoms has a pronounced minimum near 725 G, a position compatible with previously published results dealing with losses [5]. These losses are associated with a strong heating of the cloud (Fig. 3a).

Second, in figure 3 (b) for  $B \leq 675$  G, the expansion is isotropic, consistent with a collisionless regime. Here  $a$  is predicted to be  $0 \leq a \leq 55$  nm. Since  $ka \leq 0.35$ , the scattering cross section is independent of energy and the gas is not hydrodynamic ( $R \geq 1$ ). Above 700 G, a pronounced asymmetry in TOF images appears abruptly. The gas enters the hydrodynamic regime (and unitarity limit) with the same inversion of ellipticity as in Fig. 2, a signature of strong interactions. We expect that on resonance, the elastic cross section is unitarity limited for all relevant values of energy. Therefore, the maximum anisotropy, which we measure at  $B = 800(40)$  G, locates the peak of the Feshbach resonance, in agreement with the predicted position of 855(30) Gauss. A unique feature of the resonance is the very large shift ( $\simeq 80$  G) between the resonance peak and the maximum of loss and heating. This can be qualitatively explained by the

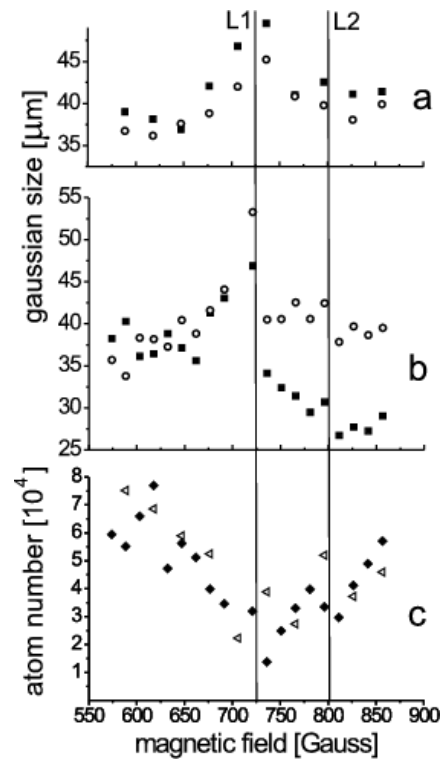


FIG. 3: a and b: Gaussian sizes along  $x$  and  $y$   $vs$  magnetic field. The detection conditions and symbols are the same as in Fig. 2. a: Expansion with  $B = 0$ . b: Expansion with  $B \neq 0$  c: Number of detected atoms  $vs$  magnetic field. Open triangles and black diamonds correspond to graph a and b, respectively. Line L1 corresponds to the maximum of loss, and L2 to the resonance position.

creation for  $a \geq 0$  of weakly bound molecules by three-body recombination. According to [28], in this process the binding energy of the molecule  $\hbar^2/ma^2$  for large  $a$ , is dissipated into kinetic energy of the atom + molecule system. For very large values of  $a$ , the binding energy is small and the heating associated with three-body recombination is negligible, and the molecules remain trapped. For small or intermediate values of  $a$ , the collision products are highly energetic, resulting in strong heating and loss. At the maximum of loss (720 G),  $a = 102$  nm and  $\hbar^2/k_B ma^2 = 7 \mu\text{K}$  is on the order of the trap depth in the weakest direction  $x$ .

As explained above, the interaction energy can be calculated directly from the difference of release energies, obtained from the gaussian sizes of Figs. 2 and 3. In Fig. 4 is plotted the ratio of interaction energy and kinetic energy  $vs$  magnetic field. As  $B$  is increased above 550 G,  $E_{int}$  first goes up, due to increasing  $a$ , in accordance with mean-field theory. Near 720 G,  $E_{int}$  changes sign abruptly. The ratio  $E_{int}/E_{kin}$  then exhibits a plateau near  $-0.12$  up to 850 G. Note that, for the data at low field (Fig. 3), the number of atoms and the temperature are not constant as a function of  $B$ . From the data at higher fields, we observe in Fig. 4 that the interaction energy becomes less and less negative above 800 G. The

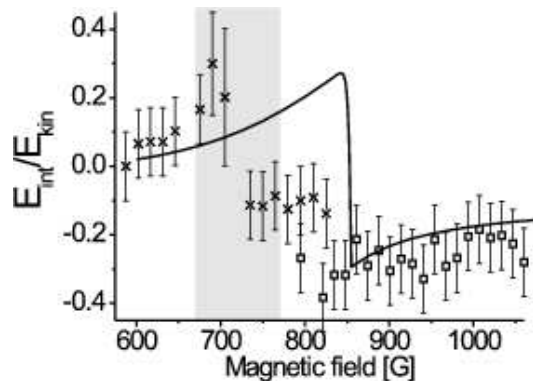


FIG. 4: Ratio of interaction energy over kinetic energy *vs* magnetic field. Open squares: atomic samples prepared above resonance as in Fig. 2. Crosses: average of three sets of data, recorded in conditions of Fig. 3. The difference between crosses and open squares in the overlap region is due to different experimental conditions described in the text. Solid line: Mean field theory calculated with a total number of atoms of  $7 \times 10^4$  and a kinetic energy of  $E_{kin}/k_B = 5.25 \mu\text{K}$ , values corresponding to the open squares conditions. The gray area indicates the region of losses.

apparent discrepancy between the two sets of data in the overlap region can be explained by different experimental conditions and, in particular, different atom numbers, temperature, and confinement. The line in Fig. 4 shows the result of a mean field calculation without any fit parameters based on a full energy dependent scattering phase shift. The mean field energy  $E_{MF}$  is then obtained from a self-consistent distribution function that contains the self-energy and trapping potential. The kinetic energy is calculated from the same distribution function. Theory and experiment agree quantitatively for  $B \geq 850 \text{ G}$  where  $a < 0$ , and for  $B \leq 720 \text{ G}$ , where  $a > 0$ . However, the observed shift between the predicted position of the resonance and the change of sign of the mean field  $720(20) \text{ G}$  is not reproduced by this theory. A possible explanation could be that dimer molecules, which are expected to be present for  $a > 0$  and close to resonance, are not part of the calculation. A large negative partial mean field contribution due to atom-molecule and molecule-molecule interactions could shift the position of the transition from positive to negative mean field.

In summary, we have studied a Fermi gas mixture in the strongly interacting regime near a Feshbach resonance. The position of the resonance is found in agreement with theoretical expectations. New features have been observed which may be the signature of richer physics, for instance molecule formation [29]. Anisotropic expansions are observed both for repulsive and attractive mean field interactions, in a moderately degenerate Fermi gas. This is interpreted in terms of collisional hydrodynamics without invoking Fermi superfluidity. Prospects for producing deeply degenerate Fermi mixtures in the superfluid state and for investigating the transition be-

tween molecular condensates and superfluid Fermi gases are promising.

We are grateful to L. Carr, Y. Castin, C. Cohen-Tannoudji, R. Combescot, J. Dalibard, D. Guéry-Odelin for useful discussions. This work was supported by CNRS, Collège de France, Region Ile de France, and EU (TMR network ERB FMRX-CT96-0002). Laboratoire Kastler Brossel is *Unité de Recherche de l'École Normale Supérieure et de l'Université Pierre et Marie Curie, associée au CNRS*.

- 
- [1] See for instance, Proc. of the Int. School of Physics "Enrico Fermi", M. Inguscio, S. Stringari, and C. Wieman eds., It. Phys. Soc. (1999)
  - [2] B. DeMarco and D. Jin, *Science* **285**, 1703 (1999).
  - [3] A. G. Truscott *et al.*, *Science* **291**, 2570 (2001).
  - [4] F. Schreck *et al.*, *Phys. Rev. Lett.*, **87**, 080403 (2001).
  - [5] K. Dieckmann *et al.*, *Phys. Rev. Lett* **89**, 203201 (2002).
  - [6] G. Modugno *et al.*, *Science* **297**, 2240 (2002).
  - [7] K. O'Hara *et al.*, *Science* **298**, 2179 (2002).
  - [8] A. G. Leggett, *J. Phys. (Paris)* **C7**, 19 (1980).
  - [9] J. Bardeen, L. Cooper and J. Schrieffer, *Phys. Rev. A* **108**, 1175 (1957).
  - [10] H. Feshbach, *Ann. Phys. (N.Y.)* **5**, 357 (1958), **19**, 287 (1962).
  - [11] E. Tiesinga, B. J. Verhaar, H. T. C. Stoof *Phys. Rev. A* **47**, 4114 (1993).
  - [12] M. Holland, S. J. J. M. F. Kokkelmans, M. L. Chiofalo and R. Walser, *Phys. Rev. Lett.*, **87** 120406 (2001).
  - [13] M. Houbiers *et al.*, *Phys. Rev. A* **57**, R1497 (1998).
  - [14] T. Loftus *et al.*, *Phys. Rev. Lett.* **88**, 173201 (2002).
  - [15] K. O'Hara *et al.*, *Phys. Rev. A*, **66**, 041401(R) (2002).
  - [16] S. Jochim *et al.*, *Phys. Rev. Lett.*, **89**, 273202 (2002).
  - [17] C. Menotti, P. Pedri, S. Stringari, *Phys. Rev. Lett.* **89**, 250402 (2002).
  - [18] We derive  $E_{rel}$  as if the whole expansion had been ballistic. Simulations of our hydrodynamic expansions show that this approximation induces a maximum error of 3%.
  - [19] Y. Kagan, E. L. Surkov, G. V. Shlyapnikov, *Phys. Rev. A*, **55**, R18 (1997).
  - [20] E. Arimondo, E. Cerboneschi, H. Wu, p. 573 in Ref. [1].
  - [21] C. A. Regal, D. Jin, E-print: cond-mat/0202246.
  - [22] I. Shvachuk *et al.*, *Phys. Rev. Lett.* **89**, 270404 (2002).
  - [23] L. Khaykovich *et al.*, *Science*, **296**, 1290-1293 (2002).
  - [24] S. Inouye *et al.*, *Nature* **392**, 151 (1998).
  - [25] In an adiabatic transformation of the gas, the phase space density is constant during the time of flight.
  - [26] In the strongly degenerate regime, this formula should be modified. See R. Combescot, E-print: cond-mat/0302209.
  - [27] G. V. Shlyapnikov, in proc. of the 18<sup>th</sup> Int. Conf. on At. Phys., H. R. Sadeghpour, D. E. Pritchard, and E. J. Heller eds., World Scientific (2002).
  - [28] D. S. Petrov, *Phys. Rev. A* **67**, 010703 (2003); L. Pricoupenko, E-print: cond-mat/0006263.
  - [29] E. A. Donley *et al.*, *Nature* **417**, 529 (2002).